

Article

Three Mathematical Models for COVID-19 Prediction

Pelayo Martínez-Fernández¹, Zulima Fernández-Muñiz¹, Ana Cernea¹, Juan Luis Fernández-Martínez¹ 
and Andrzej Kłoczkowski^{2,3,*} 

¹ Mathematics Department, Faculty of Geology, Llamaquique Campus, University of Oviedo, 33007 Oviedo, Spain

² The Steve and Cindy Rasmussen Institute for Genomic Medicine, Nationwide Children Hospital, Columbus, OH 43205, USA

³ Department of Pediatrics, The Ohio State University, Columbus, OH 43205, USA

* Correspondence: andrzej.kloczkowski@nationwidechildrens.org

Abstract: The COVID-19 outbreak was a major event that greatly impacted the economy and the health systems around the world. Understanding the behavior of the virus and being able to perform long-term and short-term future predictions of the daily new cases is a working field for machine learning methods and mathematical models. This paper compares Verhulst's, Gompertz's, and SIR models from the point of view of their efficiency to describe the behavior of COVID-19 in Spain. These mathematical models are used to predict the future of the pandemic by first solving the corresponding inverse problems to identify the model parameters in each wave separately, using as observed data the daily cases in the past. The posterior distributions of the model parameters are then inferred via the Metropolis–Hastings algorithm, comparing the robustness of each prediction model and making different representations to visualize the results obtained concerning the posterior distribution of the model parameters and their predictions. The knowledge acquired is used to perform predictions about the evolution of both the daily number of infected cases and the total number of cases during each wave. As a main conclusion, predictive models are incomplete without a corresponding uncertainty analysis of the corresponding inverse problem. The invariance of the output (posterior prediction) with respect to the forward predictive model that is used shows that the methodology shown in this paper can be used to adopt decisions in real practice (public health).

Keywords: uncertainty analysis; population models; inverse problems; COVID-19

MSC: 65Z05



Citation: Martínez-Fernández, P.; Fernández-Muñiz, Z.; Cernea, A.; Fernández-Martínez, J.L.; Kłoczkowski, A. Three Mathematical Models for COVID-19 Prediction. *Mathematics* **2023**, *11*, 506. <https://doi.org/10.3390/math11030506>

Academic Editor: Alexander B. Medvinsky

Received: 15 November 2022

Revised: 7 January 2023

Accepted: 13 January 2023

Published: 17 January 2023



Copyright: © 2023 by the authors. Licensee MDPI, Basel, Switzerland. This article is an open access article distributed under the terms and conditions of the Creative Commons Attribution (CC BY) license (<https://creativecommons.org/licenses/by/4.0/>).

1. Introduction

Mathematical models not only help us to understand the behavior of complex systems in situations that are difficult to observe but can also be of great help in predicting the future if a suitable observation dataset is available. Mathematical models in epidemiology are designed to follow the dynamics of disease transmission in groups of people. By making predictions with these models, it is possible to estimate the health needs to cope with a new outbreak of a disease, for example, the possible number of infected people, the number of ICU beds, or the number of tests to be carried out.

Different mathematical models have been used to simulate the behavior of COVID-19, ranging from those using time series that follow patterns but have difficulty predicting changes [1] to those based on artificial intelligence, which may have validity problems due to the absence of sufficient training data sets [2] and even agent-based modeling, which simulates the behavior of individuals to estimate the spread of the disease in the community [3]. These models are based on population-level parameters such as movement rates, distancing, and virus infectivity parameters, which are unknown, but there are models based on ordinary differential equations that have long been used to simulate

disease dynamics [4]. Such a model was first proposed by Kermack and McKendrick in 1927 to simulate the transmission of infectious diseases such as measles and rubella [5]. This model is known as SIR because it separates the population into three groups: the susceptible, infected, and recovered, and consists of a system of three non-linear ordinary differential equations, which has no explicit solution. However, simple calculus tools allow us to obtain a great deal of information about the solutions [6,7].

The SIR transmission model [8] considers a large, closed population with no births or natural deaths in which the rate of encounters between susceptible and infected is proportional to the size of these populations. It is a short-lived outbreak with no latent period, and recovery from infection confers permanent immunity. This requires that the members of each group are homogeneously distributed, with the probability of encounters per unit of time being the same for all individuals.

Since these assumptions are quite restrictive and, in some cases, unrealistic, the scientific community adapted the model to reality. Thus, the SEIR model incorporates the time of disease development during which an individual is affected by contagion but is not contagious to the rest of the population. SEIS is like SEIR, but immunity to the virus is never achieved. If you add a new group of people who, at the beginning of the pandemic, have passive immunity that they later lose, you obtain the MSEIR model, and if the immunity of the recovered group is temporary, it is the MSEIRS model.

Another way to model a pandemic is to treat the outbreak as a population growth model, working only with the infected group. Limited growth models, such as the logistic model proposed by Verhulst (1838) [9], can be used to understand and predict a pandemic. For small values of magnitude, at the beginning of the outbreak, the virus spreads rapidly, but as the number of infected grows, the rate of spread of the virus decreases. This is possible because measures were taken against the disease or because finding a person who has not previously been in contact with the disease becomes more difficult. The Verhulst model can predict the human population in an area with the aim of decision-making for socio-economic and demographic development [10]. Likewise, the Verhulst model, with its bounds for determining unlimited population growth [11], is a computationally reliable alternative for solving population problems [12].

Another model used in biology is that of Gompertz (1825) [13]. This model has been used mainly to describe the growth of a certain population of organisms and for the study of growing tumors [14–22]. It is a sigmoidal function describing slower growth at the beginning and end of a given period.

Fernández-Martínez et al. [23] presented the analysis of Verhulst's and Gompertz's models for the short-term and long-term prediction of the COVID-19 pandemic by solving the corresponding inverse problem via a PSO family member. In this paper, we expand this comparison to the SIR model, inferring the posterior distributions of the model parameters via the Metropolis–Hastings algorithm, which is considered a correct importance sampler.

We have compared the robustness of each algorithm, making different representations to visualize the results obtained. The knowledge acquired is applied to make predictions and obtain a range of possible variations for the evolution of both the daily number of infected cases and the total number of cases during each wave in Spain.

It is crucial to note that the approach of the three models is different, and none of them perfectly describes the context of the COVID-19 epidemic. However, this accuracy is not necessary for the calculations we are going to make in this article, and they can all be used to draw important conclusions for predicting the behavior of a pandemic (start date, end date, the peak of the wave...), leading to similar results if the data are interpreted correctly.

The following section presents the fundamentals of the SIR, Verhulst and Gompertz models. This analysis also serves to draw relevant conclusions about the dynamics of the pandemic.

2. Fundamentals of the Three Models

2.1. SIR Model

The model is governed by the following system of ordinary differential equations (ODEs):

$$\frac{dS}{dt} = -\frac{r}{K}SI \tag{1}$$

$$\frac{dI}{dt} = -\frac{r}{K}SI - \gamma I \tag{2}$$

$$\frac{dR}{dt} = \gamma I \tag{3}$$

where $r > 0$ is the transmission rate, $\gamma > 0$ the recovery rate (being the duration of infection $D = 1/\gamma$), and r/K the transmission rate. The incidence rSI/K of the number of newly infected individuals per unit of time involves individuals in the infected and susceptible classes. Additionally, the sum of Equations (1)–(3) is the derivative of the total population size, the result of which is zero. Therefore, the total population size $K = R(t) + S(t) + I(t)$ remains constant.

If each infected person has κ contacts, on average, capable of transmitting the disease per unit time, irrespective of the total population size, then $\kappa S/K$ of those contacts will be with susceptible persons. If τ of these suitable contacts result in susceptible persons, it follows that each person carrying the virus infects $\tau\kappa S/K$ susceptible people per unit of time. Therefore, defining $r = \kappa\tau$, with the parameter τ known as transmissibility, the system described above is obtained.

Taking a sufficiently large, initially susceptible population ($S(0) = K - 1$, $I(0) = 1$, $R(0) = 0$), we define the effective reproductive number $R_e = (S(0)/K)r/\gamma$ and the basic reproductive number $R_0 = r/\gamma$, then $R_e = ((K - 1)/K)r/\gamma$ is approximately equal to R_0 .

This R_e is the threshold value that determines whether a disease outbreak will die out quickly or instead spread and cause a pandemic. If $R_e \leq 1$, then $I(t)$ is a monotonic function that decreases towards zero as it grows, while if $R_e > 1$, then $I(t)$ starts growing, reaches a maximum, and finally decreases towards zero as t increases. This scenario of growing numbers of infected individuals will serve to describe an epidemic.

It is important to emphasize that the existence of a threshold for determining whether a disease outbreak becomes an epidemic or not is far from obvious and goes unnoticed by many public health and infectious disease experts. The reason is that this threshold cannot be derived from data but requires mathematical modeling.

There are some strategies for $R_e \leq 1$, such as reducing the duration of infection with antivirals, adopting strategies to reduce the number of κ contacts or τ transmissibility, and vaccinating the population to reduce the number of the initial susceptible population. Regarding the latter strategy, it is possible to avoid a pandemic by vaccinating only part of the population. This is the phenomenon known as herd immunity, and the critical vaccination threshold is achieved when the fraction of susceptible people who are vaccinated is $\rho > 1 - 1/R_e$. On the other hand, the maximum number of infected can be expressed as a function of the single parameter R_0 , as $I_{\max} = K(1 - (1/R_0)(1 + \log R_0))$.

Finally, as an epidemic progresses, the number of susceptible people and the rate at which new infections occur decreases. Eventually, $S(t)$ decreases below $\gamma K/r$, and the rate of recovery exceeds the rate of infection. Thus, $I(t)$ begins to decline, and the epidemic ends because of a lack of newly infected individuals and not for lack of the susceptible population.

2.2. Verhulst Model

Verhulst’s model falls into the class of limited growth models and is a modification of the model of Malthus (1766–1834) [24], which advocated exponential population growth. In this model, the rate of reproduction is proportional to the existing population and the

available resources and is governed by the following first-degree differential equation, representing the number of daily cases:

$$\begin{aligned} \frac{dP}{dt} &= rP\left(1 - \frac{P}{K}\right), \\ P(0) &= P_0 \end{aligned} \tag{4}$$

where $P(t)$ is the population size, which applied to epidemiology is the number of infected, r is the intrinsic growth rate, and K is the maximum population size that can be sustained by the environment, known as the carrying capacity.

The solution of Verhulst’s model is given by

$$P(t) = \frac{KP_0e^{rt}}{K + P_0(e^{rt} - 1)} \tag{5}$$

which depends on the parameters P_0 , K and r .

The maximum number of daily cases obtained is

$$\max\left(\frac{dP(t)}{dt}\right) = \frac{rK}{4}, \tag{6}$$

corresponding to $t = t_{\max} = \ln A/r$, where A is a constant that must satisfy the initial condition

$$P_0 = \frac{K}{1 + A} \tag{7}$$

Therefore, the peak of the daily infections depends on r and K , while the time at which this peak occurs depends on P_0 .

2.3. Gompertz Model

Gompertz’s model, as well as some of his new approximations, have been used in many aspects of biology, such as the growth of animals and plants or the number and volume of bacteria and cancer cells, among others [25].

There are several forms of the so-called Gompertz equation (1938) in the literature, but in this paper, we will consider the following one:

$$\begin{aligned} \frac{dP}{dt} &= rP \ln\left(\frac{K}{P}\right) \\ P(0) &= P_0 \end{aligned} \tag{8}$$

where $P(t)$, is the population at time t , r is an intrinsic growth constant, with $r > 0$, and $K > 0$, is the carrying capacity or maximum population size. The general solution is

$$P(t) = Ke^{-Be^{-rt}}, \tag{9}$$

where B represents a real constant satisfying the initial equation:

$$P(0) = Ke^{-B}. \tag{10}$$

Equation (9) can be expressed in terms of the same parameters as the Verhulst model:

$$P(t) = K\left(\frac{P_0}{K}\right)^{e^{-rt}} \tag{11}$$

The maximum number of daily cases

$$\max\left(\frac{dP(t)}{dt}\right) = \frac{Kr}{e}, \tag{12}$$

is obtained for $t_{\max} = \ln B/r$.

Identical considerations to Verhulst’s model can be made for the peak and the time at which the peak occurs. The number of infected is higher than in the case of Verhulst’s model for the same values of K and r . This result can be seen in Figures 1 and 2, in which Verhulst’s and Gompertz’s models were simulated for an initial population $P_0 = 1$ and taking different values of K and r (the same in each model).

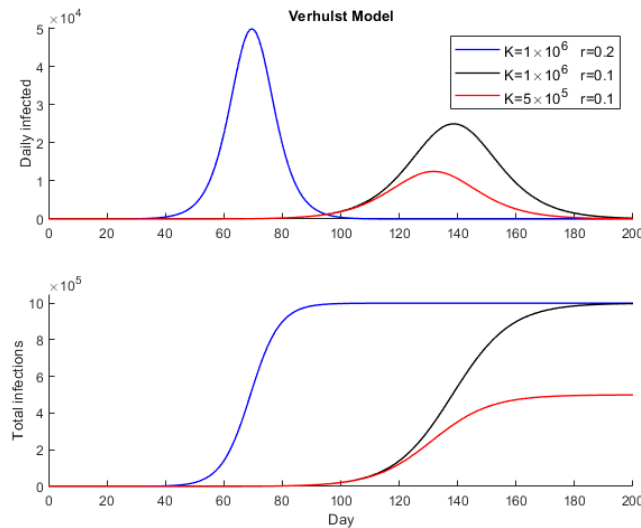


Figure 1. Epidemic simulation with Verhulst model for $P_0 = 1$.

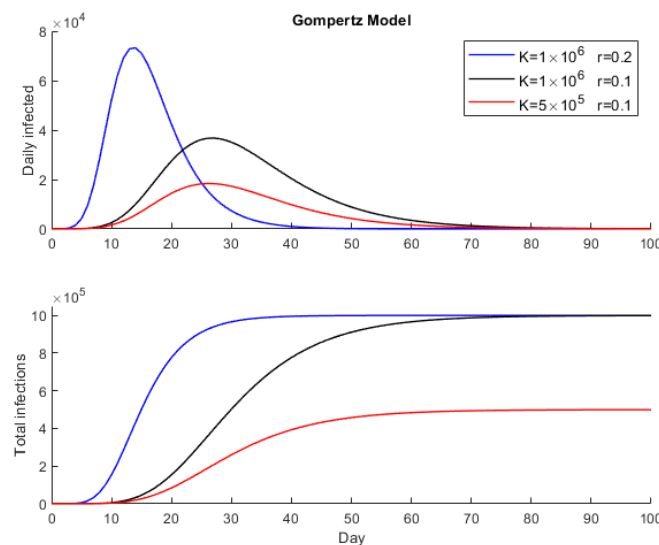


Figure 2. Epidemic simulation with Gompertz model for $P_0 = 1$.

In Verhulst’s and Gompertz’s models, the model parameters B and P_0 to K are related via a logarithmic expression. In the case of Verhulst, the logarithmic equation is

$$\ln K = \ln P_0 + B. \tag{13}$$

In the case of Gompertz’s model, from Equation (8), we obtain

$$\ln \left| \frac{dP(t)}{dt} \right| = \ln(rB) - rt, \tag{14}$$

which can be used to obtain a first approximation of r and B by linear regression.

Another possibility is taking logarithms directly in Equation (9):

$$\ln P(t) = \ln P_0 - B(e^{-rt} - 1) \tag{15}$$

and solve it for different values of t and by least squares, considering an initial value of r and obtaining the parameters P_0 and B . Analogously, least squares are used to obtain r , proceeding iteratively until the predicted value P^* satisfies that $\|P^{obs} - P^*\|_2$ is smaller than a fixed value.

3. The Inverse Problem

The inverse problem can be written in abstract form as: $\mathbf{F}(\mathbf{m}) = \mathbf{P}^{obs}$, where $\mathbf{F}(\mathbf{m})$ represents the predicted time series with the parameters obtained by the corresponding model (Verhults or Gormpertz), $\mathbf{P}^{obs} = (P_1, P_2, \dots, P_n) \in N^n$ are the observed data (infected people) in times t_1, t_2, \dots, t_n , and \mathbf{m} are the model parameters of the prediction problem. For instance, in the Verhulst model $\mathbf{m} = (K, P_0, r)$, which are the parameters that we need to identify to perform the ad-future predictions.

The data of our problem is a time series containing the number of total infected on each measurement day, so the inverse problem is to find a set of parameters $\mathbf{m} = (K, P_0, r)$ such as the prediction error:

$$E_1(\mathbf{m}) = \frac{\|\mathbf{F}(\mathbf{m}) - \mathbf{P}^{obs}\|_1}{\|\mathbf{P}^{obs}\|_1} \tag{16}$$

is less than a certain tolerance tol , where $\mathbf{F}(\mathbf{m})$ represents the predicted time series with the parameters obtained by the corresponding model.

The main source of noise in data, in this case, is the number of infected people, which sometimes corresponds to two consecutive days instead of the same. This is due to the way that the data were transmitted. Additionally, sometimes the criteria to classify the infections has changed over time, causing some data incongruences. Additionally, COVID-19 cases are usually undercounted. All these facts make it so the model should be a useful approximation of reality (noise included) to optimize decision-making. The fact that the L1 norm is used has some implications for the statistical distribution of the outliers due to its robustness in their presence.

The set of models that fit the data with an error smaller than tol contains the so-called equivalent models

$$M_{tol} = \{\mathbf{m} : E(\mathbf{m}) \leq tol\} \tag{17}$$

which can be found in a curvilinear valley or even in different unconnected basins [26]. In this case of a set of plausible values, uncertainty analysis is necessary to obtain a representative sample of the solutions, which will be carried out by a method capable of exploring the set of equivalent parameters to obtain the most plausible one. This method is a member of the PSO (Particle Swarm Optimization) family called RR-PSO (Regressive-Regressive Particle Swarm Optimization), designed by Fernandez-Martinez and Garcia Gonzalo [27]. It is important to note in this case that casting the inverse problem as a sampling problem makes the use of regularization unnecessary. The only prior information that is used is the search space where the model parameters are sampled. The use of the Metropolis–Hastings (MH) algorithm corresponds to a Bayesian formulation of the inverse problem, while the sampling of the parameters through an exploratory global algorithm, such as RR-PSO, is only a numerical approximation of the posterior distribution of the model parameters provided by a correct theoretical sampler, like MH.

4. Results

The data were obtained from reports provided by the Centro de Coordinacion de Alertas y Emergencias Sanitarias del Ministerio de Sanidad del Gobierno de España [28].

After obtaining the data on total infections and computing the daily infections, the next step of our study was to set the start and end dates of each wave. As can be seen in Figure 3, the first wave was the smallest, but in reality, it is believed that there were quite a few more infections than reported by health authorities.

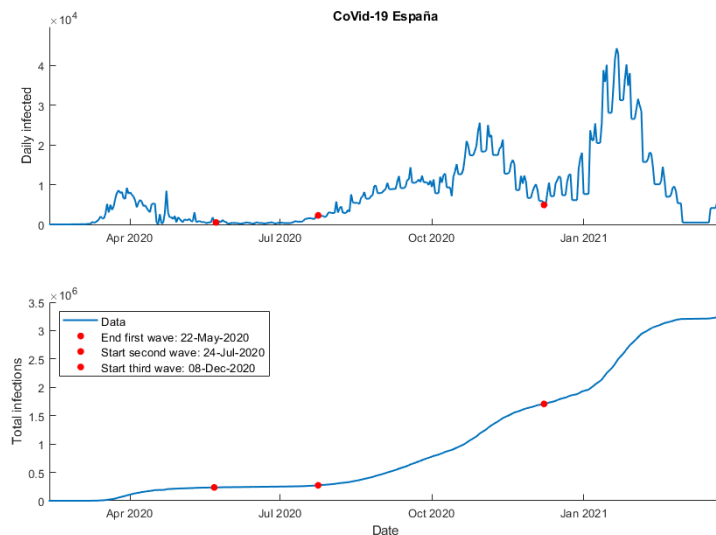


Figure 3. Data COVID-19 Spain (Updated: 25 March 2021).

For the purpose of this article, we will focus our attention on the third wave, which starts around 8th December 2020 and is characterized by an upturn in the daily cases a few days after the Christmas holidays (see [23] for more information).

4.1. Results Comparison

First, using the Verhulst model, really good results have been obtained, which can be found in Figure 4, where the red dashed line is the observed data and the green one is the best model obtained by minimizing the error. The error obtained was 1.76% with an initial infected population of approximately $P_0 \approx 3 \times 10^4$, a carrying capacity $K \approx 1.55 \times 10^6$, and a growth rate $r = 0.086$.

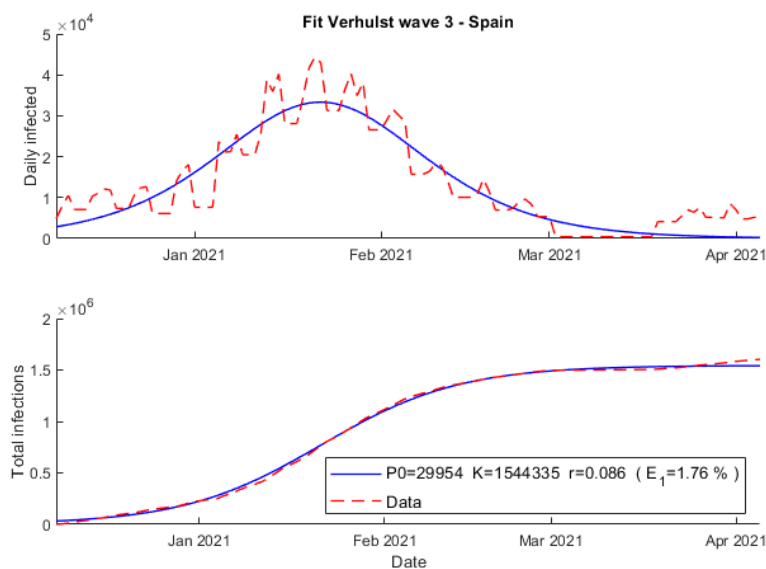


Figure 4. Fit using Verhulst model wave 3 COVID-19 Spain.

Second, Figure 5 shows how the fit obtained using Gompertz’s model failed primarily at the beginning of the outbreak, with an error of 3.98%. Furthermore, the initial population obtained, $P_0 = 16$, has been much different with respect to the Verhulst results, and the growth rate is slightly lower, $r = 0.062$.

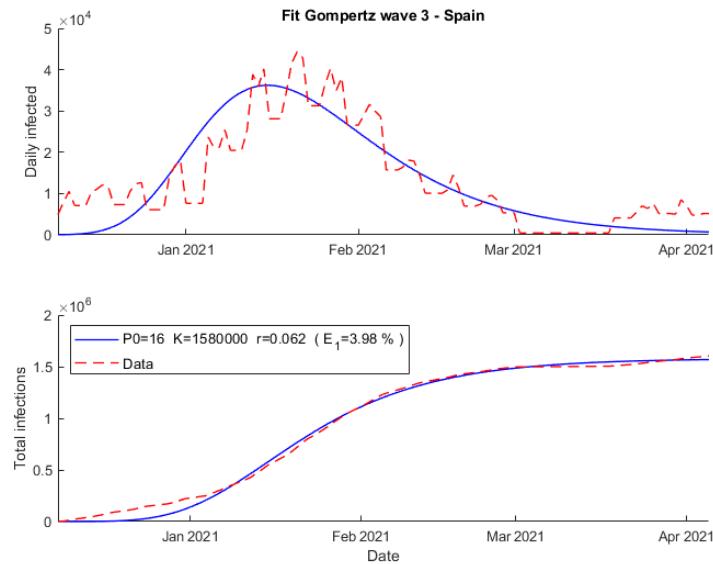


Figure 5. Fit using Gompertz’s model wave 3 COVID-19 Spain.

Finally, the SIR model returns a precise fit, which can be seen in Figure 6, with an error of 2.15%, a growth rate of $r = 0.255$ and a recovery rate of 0.161. It is important to note that, unlike Verhulst’s and Gompertz’s fits, the SIR model does not need to reach the carrying capacity, $K \approx 2.5 \times 10^6$, at the end of an outbreak. This could be visualized in Figure 7, where the epidemic ends because of a reduction in the number of infected people and not due to the lack of susceptibility.

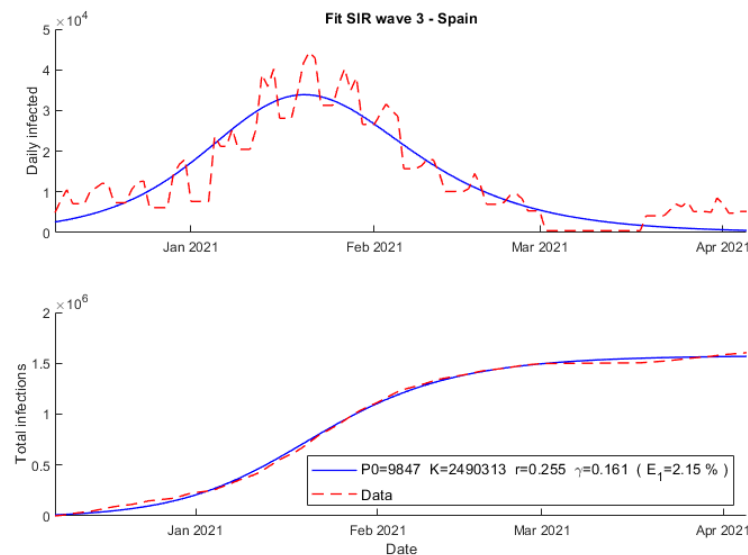


Figure 6. Fit using SIR model wave 3 COVID-19 Spain.

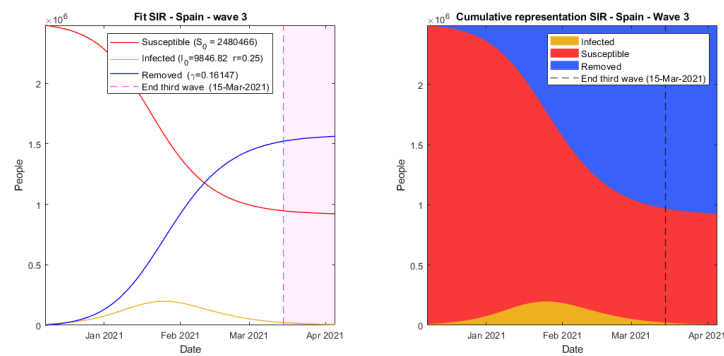


Figure 7. Simulation using SIR model wave 3 COVID-19 Spain.

4.2. Predictions

In order to make predictions, it is first necessary to obtain a representative sample of equivalent models. In this paper, the Metropolis–Hastings algorithm, which is a Markov chain Monte Carlo (MCMC) method, was chosen.

After sampling, the next step is to extrapolate the pandemic curves and calculate the different percentiles. The p-percentile of a prediction on one day is the number of infected people left by the p% of predictions below.

With the aim of giving a general idea about the effectiveness of the different models at making predictions, two examples of it will be presented, the first one made on 5 January 2021 and the second one on 25 January, a few days after the peak of the wave in daily cases.

On the one hand, as it may be seen in Figures 8–10, the 75th and 90th Verhulst percentiles are the only ones that correctly predict the fast growth of daily infections at the beginning of the outbreak.

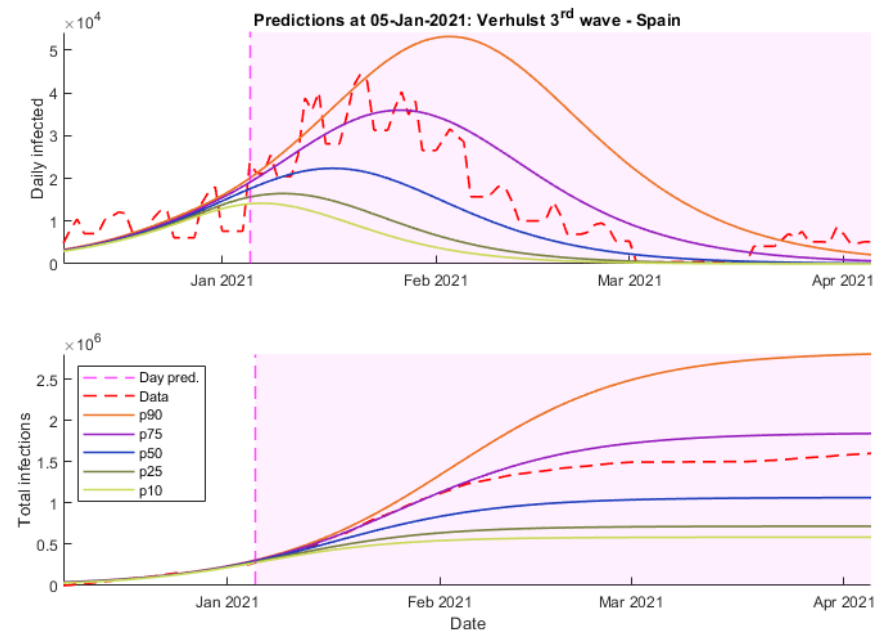


Figure 8. Predictions 5 January 2021 wave 3 Verhulst—Spain.

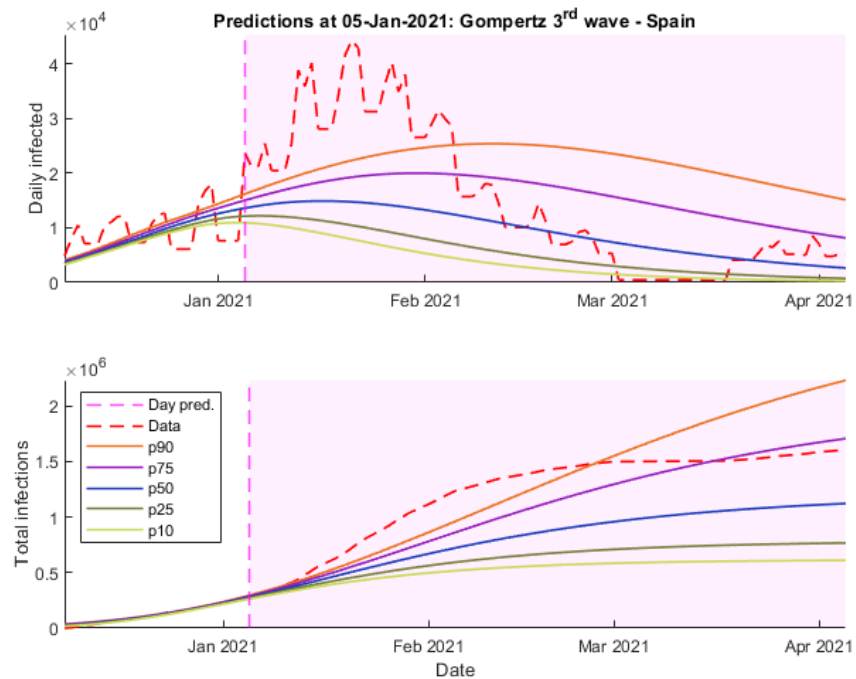


Figure 9. Predictions 5 January 2021 wave 3 Gompertz—Spain.

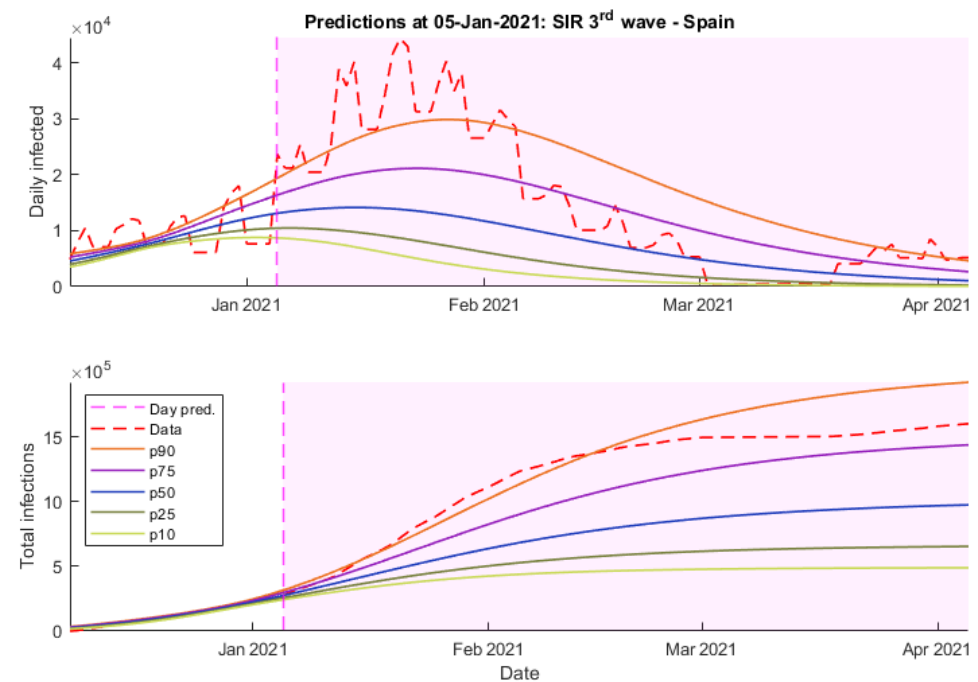


Figure 10. Predictions 5 January 2021 wave 3 SIR—Spain.

On the other hand, they fail at predicting the end of the outbreak, whereas other models like SIR obtain more accurate predictions. In this case, Gompertz’s model seems like it has not been able to detect the tendency properly due to the lack of data.

Continuing with the predictions made on 25 January, it can be seen how all the models considerably improved their results.

Figures 11–13 show the predictions of these three models. For instance, the Verhulst and SIR models (Figures 11 and 13) not only allow us to obtain a more precise frame of daily cases, but they fit the wave shape much better.

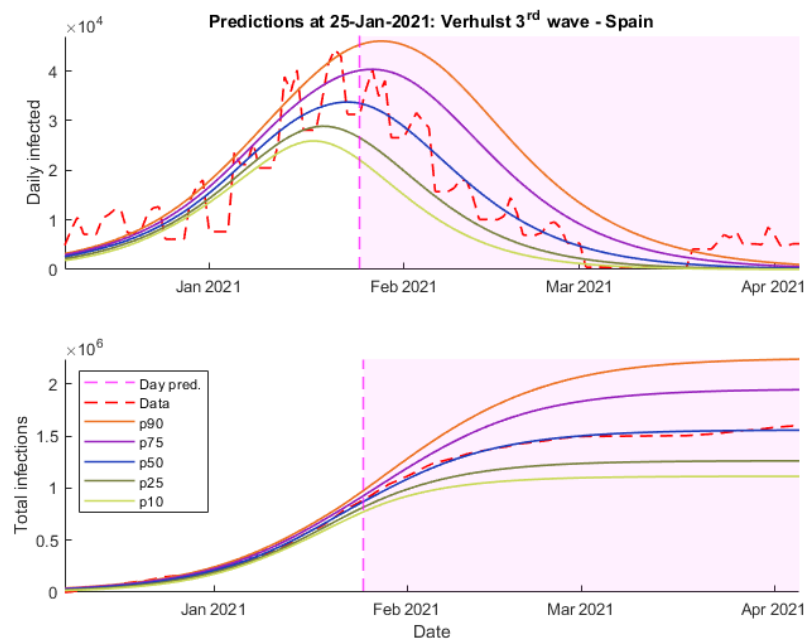


Figure 11. Predictions 25 January 2021 wave 3 Verhulst—Spain.

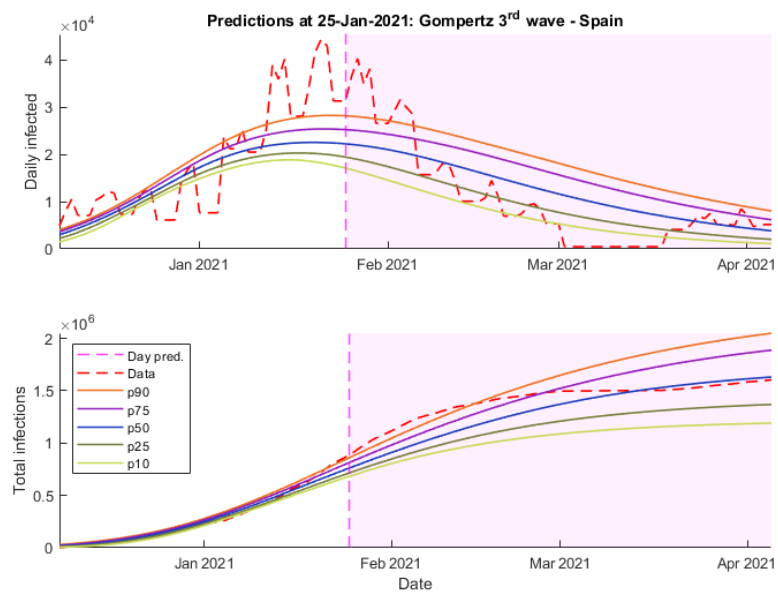


Figure 12. Predictions 25 January 2021 wave 3 Gompertz—Spain.

Finally, as can be seen in Figure 12, Gompertz’s predictions maintain that long-term trend that fails to adjust the peak of the wave but is the most accurate when it comes to predicting the number of daily cases over April.

To complement these results, Appendix A shows the posterior histograms of the model parameters for each of the models and COVID-19 waves. These histograms account for the uncertainty analysis (model appraisal) of the inverse unknowns: initial population, growth rate, maximum population infected (in the case of Verhulst’s and Gompertz’s models), and for the SIR parameters via the Metropolis–Hastings algorithm. As can be observed, all the models provide very consistent results. Therefore, the conclusions achieved by the posterior analysis are similar.

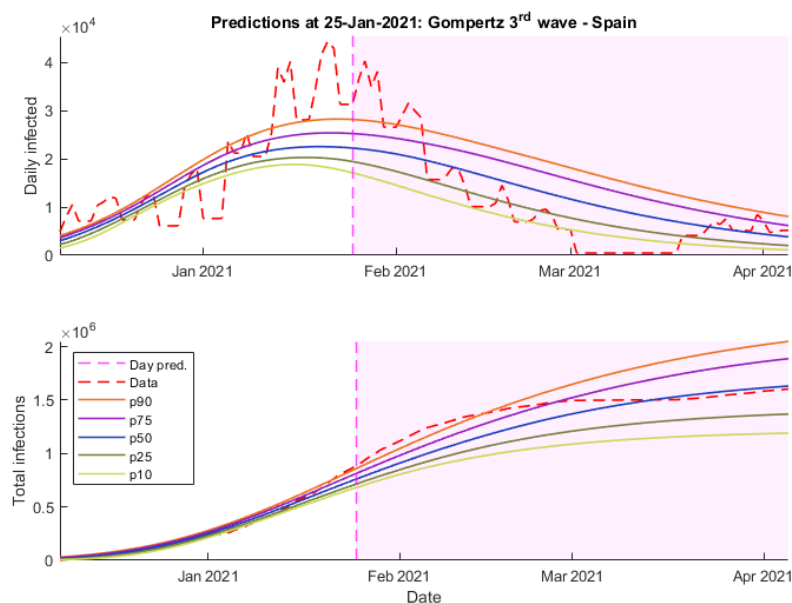


Figure 13. Predictions 25 January 2021 wave 3 SIR—Spain.

5. Conclusions

In this article, a comparison is made between Verhulst's, Gompertz's, and SIR models in terms of their effectiveness in predicting the effects of COVID-19 outbreaks in Spain and for the purpose of socio-health planning. The analysis of the different solutions obtained by each model shows the daily prediction of infected people and the total number of infections. All this translates into reliable present and future predictions that are key in determining health measures aimed at the population to mitigate the most serious effects of the next wave.

We show different predictions for COVID-19 in Spain made by each of the models, where the infection rate is between 3% and 10%, i.e., the virus infects between 3 and 10 people out of 100 vulnerable people. The three models show similar results, but it is easier to refine the parameters of Verhulst's model. In view of these facts, it would be more appropriate to use the Verhulst model for long-term forecasts and the SIR model for short-term forecasts or when precise information on the recovery rate is available. Finally, it is clear throughout the article that none of the models is perfect, but precisely because of these differences in the predictions of each model, they could be used in a complementary way to inform decision-making during a pandemic.

Author Contributions: P.M.-F., Z.F.-M. and J.L.F.-M. developed the algorithms used in this paper. A.C., A.K., P.M.-F., Z.F.-M. and J.L.F.-M. have participated in the numerical analysis, interpretation, and scientific writing of the paper. All authors have read and agreed to the published version of the manuscript.

Funding: This research received no external funding.

Data Availability Statement: The data were obtained from reports provided by the Centro de Coordinacion de Alertas y Emergencias Sanitarias del Ministerio de Sanidad del Gobierno de España.

Conflicts of Interest: The authors declare no conflict of interest.

Appendix A Appendix A

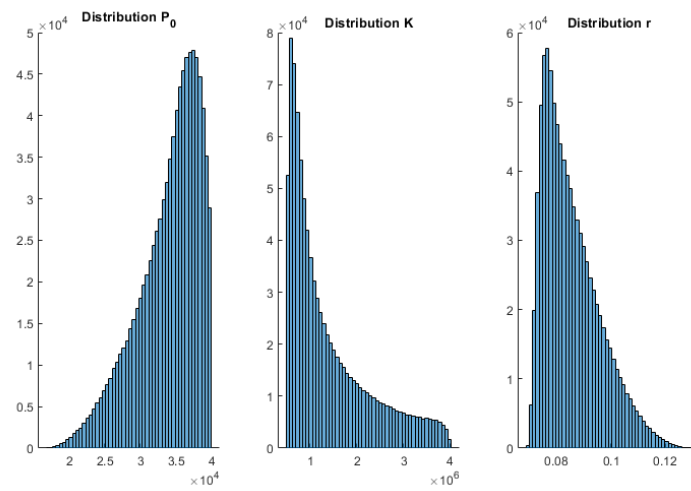


Figure A1. Histograms 5 January 2021 wave 3 Verhulst—Spain.

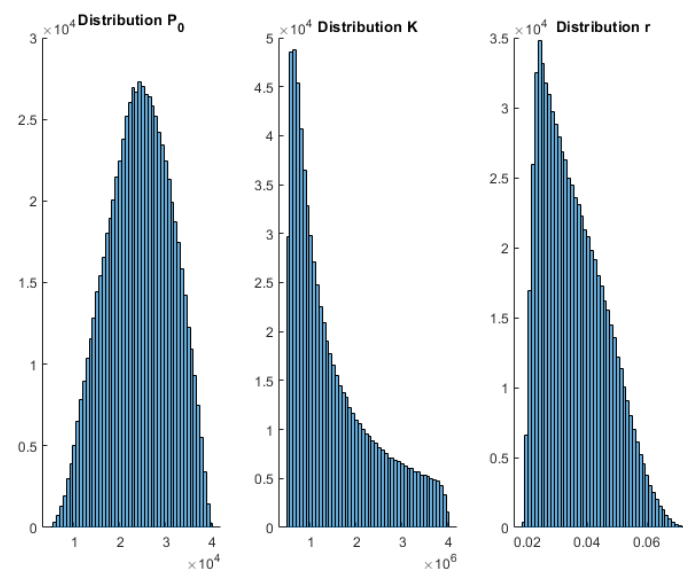


Figure A2. Histograms 5 January 2021 wave 3 Gompertz—Spain.

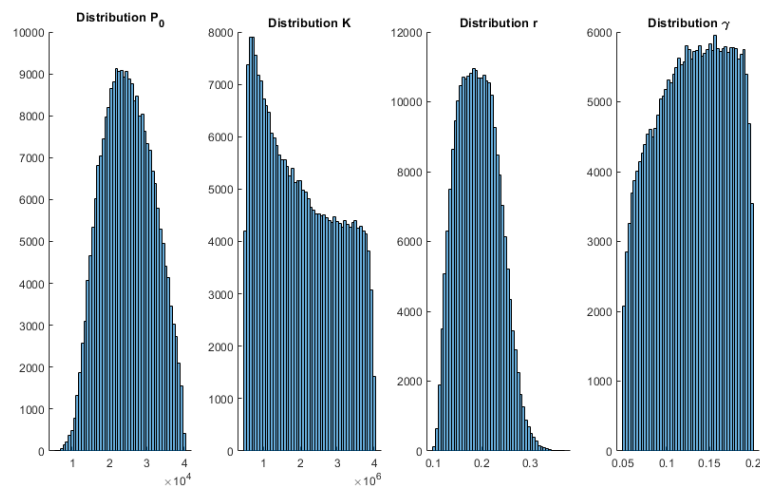


Figure A3. Histograms 5 January 2021 wave 3 SIR—Spain.

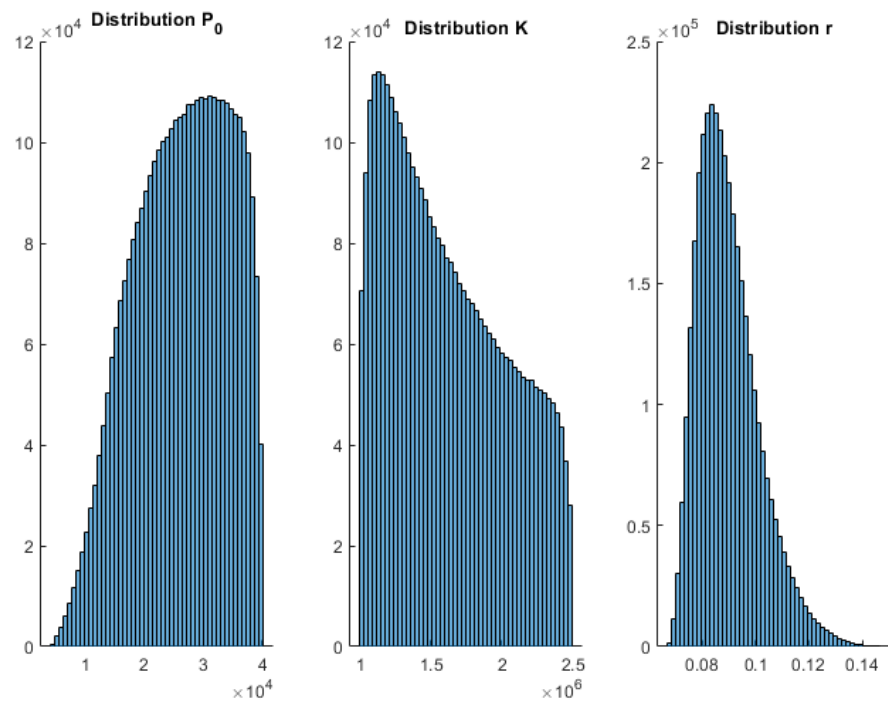


Figure A4. Histograms 25 January 2021 wave 3 Verhulst—Spain.

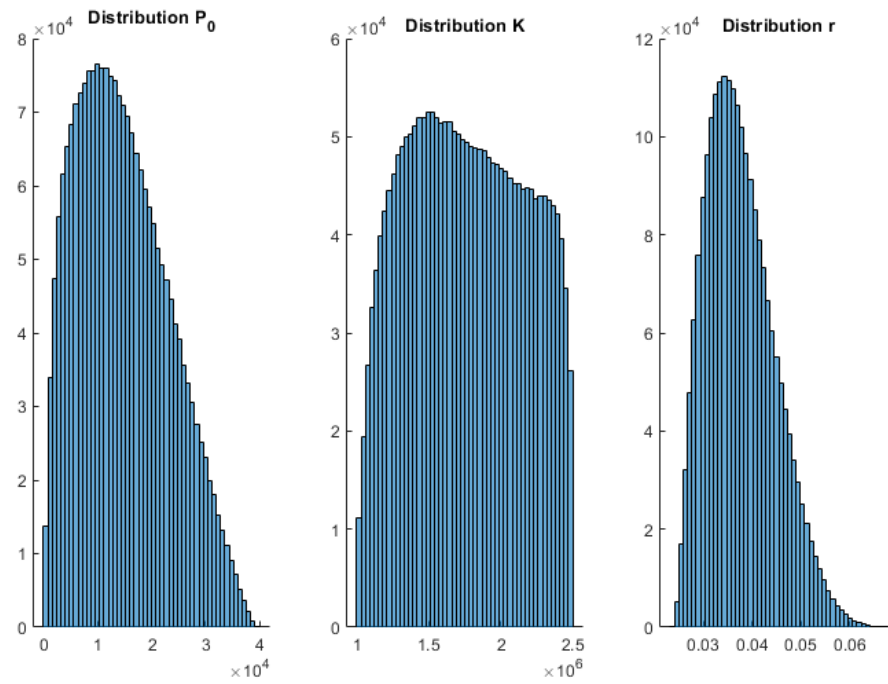


Figure A5. Histograms 25 January 2021 wave 3 Gompertz—Spain.

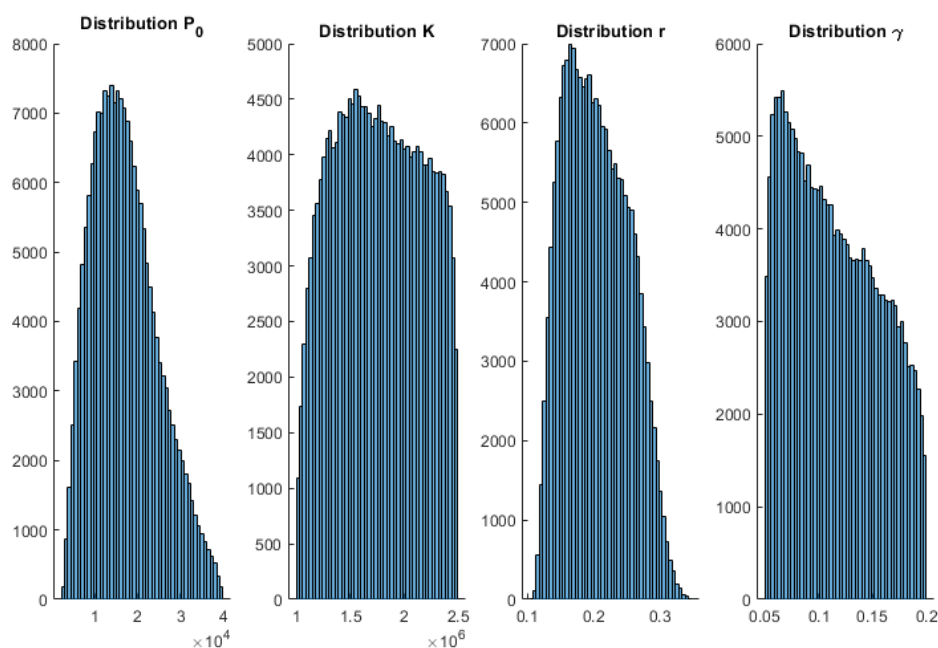


Figure A6. Histograms 25 January 2021 wave 3 SIR—Spain.

References

1. Elmousalami, H.H.; Hassanien, A.E. Day level forecasting for coronavirus disease (COVID-19) spread: Analysis, modeling and recommendations. *arXiv* **2020**, arXiv:2003.07778.
2. Hu, Z.; Ge, Q.; Jin, L.; Xiong, M. Artificial intelligence forecasting of covid-19 in China. *arXiv* **2020**, arXiv:2002.07112. [[CrossRef](#)]
3. Kim, Y.; Ryu, H.; Lee, S. Agent-based modeling for super-spreading events: A case study of MERS-CoV transmission dynamics in the Republic of Korea. *Int. J. Environ. Res. Public Health*. **2018**, *15*, 2369. [[CrossRef](#)] [[PubMed](#)]
4. Satsuma, J.; Willox, R.; Ramani, A.; Grammaticos, B.; Carstea, A. Extending the SIR epidemic model. *Phys. A Stat. Mech. Appl.* **2004**, *336*, 369–375. [[CrossRef](#)]
5. Bacaër, N. *A Short History of Mathematical Population Dynamics*; Nicolas, B., Ed.; Springer: London, UK, 2011; pp. 89–96.
6. Britton, T. Stochastic epidemic models: A survey. *Math. Biosci.* **2010**, *225*, 24–35. [[CrossRef](#)]
7. Zhou, Y.; Ma, Z.; Brauer, F. A Discrete epidemic model for SARS transmission and control in China. *Math. Comput. Model.* **2004**, *40*, 1491–1506. [[CrossRef](#)]
8. Kermack, W.O.; McKendrick, A.G. A contribution to the mathematical theory of epidemics. In Proceedings of the Royal Society of London, Serie A Containing Papers of Mathematics and Physical Character, London, UK, 2 May 1927; Volume 115, pp. 700–721.
9. Verhulst, P.F. Notice sur la loi que la population suit dans son accroissement. *Corresp. Mathématique Phys.* **1838**, *10*, 113–121.
10. Dawed, M.Y.; Koya, P.R.; Goshu, A.T. Mathematical Modelling of Population Growth: The Case of Logistic and Von Bertalanffy Models. *Open J. Model. Simul.* **2014**, *2*, 113–126. [[CrossRef](#)]
11. Hillen, T. Applications and Limitations of the Verhulst Model for Populations. *Math Biol.* **2003**, *6*, 19–20.
12. Sunday, J.; James, A.; Ibjola, E.; Ogunrinde, R.; Ogunyebi, S.A. Computational Approach to Verhulst-Pearl Model. *IOSR J. Math.* **2012**, *2*, 45–52. [[CrossRef](#)]
13. Gompertz, B. On the nature of the function expressive of the law of human mortality, and on a new mode of determining the value of life contingencies. *Philos. Trans. R. Soc. Lond. B Biol. Sci.* **1825**, *182*, 513–585.
14. Altrock, P.M.; Liu, L.L.; Michor, F. The mathematics of cancer: Integrating quantitative models. *Nat. Rev. Cancer* **2015**, *15*, 730–745. [[CrossRef](#)]
15. Barbolosi, D.; Ciccolini, J.; Lacarelle, B.; Barlesi, F.; André, N. Computational oncology—mathematical modelling of drug regimens for precision medicine. *Nat. Rev. Clin. Oncol.* **2016**, *13*, 242–254. [[CrossRef](#)]
16. Benzekry, S.; Lamont, C.; Beheshti, A.; Tracz, A.; Ebos, J.M.L.; Hlatky, L.; Hahnfeldt, P. Classical mathematical models for description and prediction of experimental tumor growth. *PLOS Comput. Biol.* **2014**, *10*, e1003800. [[CrossRef](#)]
17. Laird, A.K. Dynamics of tumor growth. *Br. J. Cancer* **1964**, *18*, 490–502. [[CrossRef](#)]
18. Paine, C.E.T.; Marthews, T.R.; Vogt, D.R.; Purves, D.; Rees, M.; Hector, A.; Turnbull, L.A. How to fit nonlinear plant growth models and calculate growth rates: And update for ecologists. *Methods Ecol. Evol.* **2012**, *3*, 245–256. [[CrossRef](#)]
19. Ricker, W.E. Growth rates and models. In *Fish Physiology*; Hoar, W.S., Randall, D.J., Brett, J.R., Eds.; Academic Press: London, UK, 1979; pp. 677–743.
20. Skinner, G.E.; Larkin, J.W. Mathematical modeling of microbial growth: A review. *J. Food Saf.* **1994**, *14*, 175–217. [[CrossRef](#)]
21. Winsor, C.P. The Gompertz curve as a growth curve. *Proc. Nat. Acad. Sci. USA* **1932**, *18*, 1–8. [[CrossRef](#)]

22. Zwietering, M.H.; Jongenburger, I.; Rombouts, F.M.; Van'T Rie, T.K. Modeling of the bacterial growth Curve. *Appl. Env. Microbiol.* **1990**, *56*, 1975–1981. [[CrossRef](#)]
23. Fernández-Martínez, J.L.; Fernández-Muñiz, Z.; Cernea, A.; Kloczkowski, A. Predictive Mathematical Models of the Short-Term and Long-Term Growth of the COVID-19 Pandemic. *Comput. Math. Methods Med.* **2021**, *2021*, 5556433. [[CrossRef](#)]
24. Malthus, T.R. An essay on the principle of population, as it affects the future improvement of society. First edition with remarks on the speculations of Mr. Godwin, M. Condorcet, and other writers. 1798. Available online: <http://www.esp.org/books/malthus/population/malthus.pdf> (accessed on 6 January 2023).
25. Tjørve, K.M.C.; Tjørve, E. The use of Gompertz models in growth analyses, and new Gompertz-model approach: An addition to the Unified-Richards family. *PLoS ONE* **2017**, *12*, e0178691. [[CrossRef](#)] [[PubMed](#)]
26. Fernández-Martínez, J.L.; Fernández-Muñiz, M.Z.; Tompkins, M.J. On the topography of the cost functional in linear and nonlinear inverse problems. *Geophysics* **2012**, *77*, W1–W15. [[CrossRef](#)]
27. Fernández-Martínez, J.L.; García-Gonzalo, E. Stochastic stability and numerical analysis of two novel algorithms of the PSO family: PP-GPSO and RR-GPSO. *Int. J. Artif. Intell. Tools* **2012**, *21*, 1240011. [[CrossRef](#)]
28. Centro de Coordinación de Alertas y Emergencias Sanitarias. Ministerio de Sanidad. Gobierno de España. Actualización COVID-19. Available online: https://www.mscbs.gob.es/profesionales/saludPublica/ccayes/alertasActual/nCov/documentos/Actualizacion_365_COVID-19.pdf (accessed on 30 April 2021).

Disclaimer/Publisher's Note: The statements, opinions and data contained in all publications are solely those of the individual author(s) and contributor(s) and not of MDPI and/or the editor(s). MDPI and/or the editor(s) disclaim responsibility for any injury to people or property resulting from any ideas, methods, instructions or products referred to in the content.